Optics Letters

Demonstration of on-chip quantum dot microcavity lasers in a molecularly engineered annular groove

Cong Chen,[1,2,†] Jin Yuan,[3,†] Lei Wan,[1,8] Hengky Chandrahalim,[4,9] Zhenshi Chen,[1] Naoya Nishimura,[5] Harunobu Takeda,[2] Hiroaki Yoshioka,[2] Weiping Liu,[1] Yuji Oki,[2] Xudong Fan,[6] and Zhaohui Li[7,10]

[1]Department of Electronic Engineering, College of Information Science and Technology, Jinan University, Guangzhou 510632, China
[2]Graduate School and Faculty of Information Science and Electrical Engineering, Kyushu University, Fukuoka 819 0395, Japan
[3]Institute of Lightwave Technology, Beijing Jiaotong University, Beijing 100044, China
[4]Department of Electrical and Computer Engineering, The Air Force Institute of Technology, Wright-Patterson AFB, Ohio 45433, USA
[5]Nissan Chemical Corporation, 488-6, Suzumi-cho, Funabashi 274-0052, Japan
[6]Department of Biomedical Engineering, University of Michigan, Ann Arbor, Michigan 48109, USA
[7]State Key Laboratory of Optoelectronic Materials and Technologies and School of Electronics and Information Technology, Sun Yat-Sen University, Guangzhou 511400, China
[8]e-mail: wanlei@jnu.edu.cn
[9]e-mail: hengky.chandrahalim@afit.edu
[10]e-mail: lzhh88@mail.sysu.edu.cn

Received 4 December 2018; revised 15 December 2018; accepted 15 December 2018; posted 17 December 2018 (Doc. ID 354486); published 16 January 2019

The on-chip quantum dot (QD) microcavity laser engineered on an annular groove made of fused silica was demonstrated based on the external quasi-cavity configuration. By incorporating an appropriate dose of polymer into QD film, the spectral purity of the lasing spectrum was significantly enhanced. In contrast to the dye microcavity laser embedded on the same trench profile, a QD laser possesses a lifetime that is over 10 times longer. We have introduced a unique two-step quantum gain deposition process that has remarkably reduced the wavelength drifts of laser emissions in an aqueous environment by approximately 400%. The reconfigurable cavity platform in combination with an appropriately engineered quantum gain medium embedded onto it promises to enable photostable chip-scale coherent light sources for various photonic, chemical, and biochemical sensing applications.

https://doi.org/10.1364/OL.44.000495

Engineering of quantum dot (QD) microcavity lasers has attracted enormous attention since visible light lasing enabled by single-exciton gain in colloidal QD films was demonstrated by Dang *et al.* [1]. During studies of QD lasing behaviors, the combination of whispering-gallery mode (WGM) microcavities and QD gain media is usually preferred due to the advantages of facile fabrications, high quantum yields, tunable emission wavelengths, and solution-processable features of the QD films [2]. Three main fabrication methods are generally used to realize WGM-based QD microcavity lasers.

The first method is based on an external cavity configuration, a traditional method driven by low-concentration QDs as the exterior coating. The principle mechanism of lasing is amplification of luminescence from the QD coating coupled into the WGM resonators with high-quality (high-Q) factors ($>10^7$) via evanescent fields. The typical configurations are QD-coated microsphere and microtoroidal cavities, for which the WGMs lasing properties have been demonstrated by Snee *et al.* [3] and Min *et al.* [4]. However, to realize low-threshold lasing, WGM microcavities with ultrahigh-Q factors are mandatory, which in no doubt increases the fabrication complexities of the QD lasers.

The second fabrication technique is based on an external cavity-free configuration, which is an emerging method enabled by high-concentration QD film as both the microcavity and gain medium body. The primary mechanism is the formation of the self-assembled microcavity configuration in the QD film under the functions of exterior stress or stain. For instance, Feber *et al.* reported that they used pure QDs filled into the pre-treated silicon template with a ring trench width of 500 nm and depth of 500 nm as the matrix of the microring laser, which allowed them to strip off the ring QDs as the core layer from the silicon template using ultraviolet-light-curable epoxy as a cladding layer [5]. In addition, Wang *et al.* presented a WGM-QD microbubble laser realized by drop-casting high-concentration QD/PMMA nanocomposite based on an evaporated colloidal QD droplet and stability of the polymer [6] and microdisk laser by the ink-jet printing technique based on the coffee-ring effect [7]. Rong *et al.* demonstrated an on-chip QD microplate laser using the water-dripping method based on

surface tension and stress relaxation phenomena [8]. The facile fabrications have introduced diversity of the WGM-based QD microcavity lasers. Thus, many more fabrication approaches and microcavity configurations are expected to trigger exploration of the on-chip integrated QD microcavity laser.

The last fabrication method is based on an external quasi-cavity configuration, which is done by infusing a gain medium to a carrier material and then embedding the mixture into a microcavity host that also serves as a cladding. The fundamental mechanism of the device is the conformal adhesion of the QDs or nanocomposite gain media as the core layer around the patterned microcavity host. As a proof of concept, Kiraz *et al.* reported the optofluidic laser by combining silica capillary and self-assembled monolayer QD film adhered on the inner wall of the capillary [9]. This demonstration has motivated us to explore the possibility of realizing QD lasers on a chip.

In response to this pursuit, we have designed and characterized a prototype of the on-chip QD microcavity laser by the annular groove etched into the fused-silica substrate with relatively large dimensions. This chemically, mechanically, and thermally stable annular groove platform has opened possibilities to realize different emissive reconfigurable quantum and molecular gain media on a chip-scale microcavity. As a flexible on-chip QD microcavity laser, the lasing behaviors in different environments were characterized to show their potential in sensing applications.

The QD laser was fabricated on a fused-silica wafer as a cladding layer with an annular groove partially deposited with a cured pure colloidal CdSe/ZnS core-shell QD (size: 8 nm) or polystyrene-doped (PS-doped) QD film as a core layer. Here, the PS as a dopant was chosen due to its high refractive index (RI) compared with common polymers. For the pure QD laser, 30 mg/mL QDs dispersed in toluene were spin-coated onto the patterned wafer at a low speed and cured on a hot-plate at 130° C for 15 min. The RI of QD film was estimated to be 2.45 [10]. For the PS-doped QD laser, the mixture of the PS solution (3 wt. %) and pure QDs mentioned above by volume ratio of 1:9 was similarly spin-coated on the wafer. Figure 1(a) shows the scanning electron microscope (SEM) image of an etched ring resonator host. The detailed fabrication was discussed in our previous work [11]. In this work, the fabrication processes of the lasers are plotted in Figs. 1(b)–1(d). The top and cross-sectional views are illustrated in Fig. 1(e).

The excitation and readout of the lasing signals for the on-chip QD microcavity laser were completed by a micro-photoluminescence (μ-PL) system. Figure 2 shows the schematic

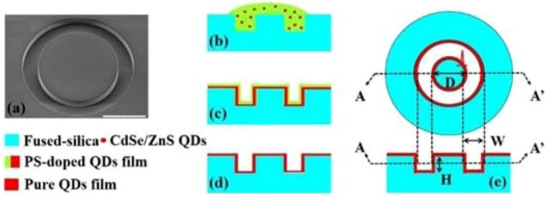

Fig. 1. (a) SEM image of an etched fused-silica substrate with an annular groove. The width (W) and height (H) of this annular groove were 40 μm and 30 μm, respectively. The diameter (D) of the inner disk was 160 μm. (b)–(d) Cross-sectional views corresponding to PS-doped QDs (b) dripped, (c) spin-coated, and (d) pure QDs cured on the patterned wafer. (e) Top view and cross-sectional view along the AA' plane of a QD microcavity laser. Scale bar: 100 μm.

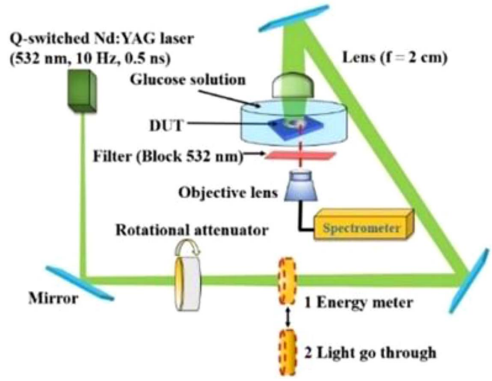

Fig. 2. Schematic of the measurement setup for the on-chip QD microcavity laser in different environments.

of the μ-PL system. Optical excitation was generated using a frequency-doubled Nd:YAG pulsed laser ($\lambda = 532$ nm, PNG-002025-040, Nanolase Corp.) via free-space coupling. The pulse width and repetition rate were 0.5 ns and 10 Hz, respectively. The pump source (300-μm-diameter light spot) was focused on the QD laser using a planoconvex lens with a focal length of 2 cm. Under the optical microscope system (Eclipse TE2000-U, Nikon), the lasing signal was collected from the bottom-side edge of the laser by a multimode fiber (Thorlabs, FP600ERT, core diameter: 200 μm). The laser emission in the direction orthogonal to the resonator plane (due to scattering on structural defects in the cavity) was aligned to a multimode fiber in a way that minimized the PL background. The collected lasing signals were recorded by a grating spectrometer (MS7504, Solar TII), which used the exposure time of 1 s. The device under test (DUT) was placed into a plastic petri dish, which can be used to characterize the performance of the laser in different environments.

Based on the above measurement setup, the spectra and thresholds of both QD microcavity lasers were characterized using 1200 l/mm grating. A plot in Fig. 3(a) shows the spectrum of a pure QD laser at a pump intensity of 16 μJ/mm^2,

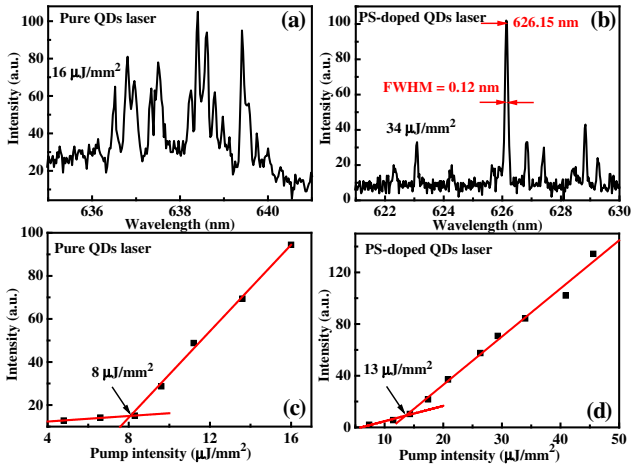

Fig. 3. Lasing spectra of (a) pure and (b) PS-doped QD microcavity lasers with excitation intensity of 16 μJ/mm^2 and 34 μJ/mm^2, respectively. Lasing threshold curves corresponding to (c) pure and (d) PS-doped QD microcavity lasers.

which was twice threshold [8 μJ/mm^2 in Fig. 3(c)]. Herein the integrated intensities of lasing spectra from 636 nm to 640 nm obtained at the different pump intensities were used to estimate the lasing threshold. In Fig. 3(a), lasing spectrum broadening was observed, caused mainly by overlapping of multiple modes. Specific modes are difficult to identify, as they partly originate from the scattering of rough sidewalls of the pure QD microcavity that facilitates the appearance of several disordered lasing modes. In addition, the cracked QD film due to the high concentration also introduced undesired scatterings. For the PS-doped QD laser, the spectrum was recorded at pump intensity of 34 μJ/mm^2, which was 2.6-fold threshold (13 μJ/mm^2), as shown in Figs. 3(b) and 3(d). Herein the peak intensities of the laser emission around 626.15 nm at the different pump intensities were used to reveal the lasing threshold. The uncertainty of the pump intensity for all experiments was within ~0.28 μJ/mm^2. The spectrum of the PS-doped QD laser exhibited better spectral purity compared to that of the pure QD laser. This indicates that the addition of PS has made the cavity's sidewall smoother and has also suppressed the undesired scattering. In fact, the lasing spectrum with high purity is favorable for many sensing applications. The full width at half maximum (FWHM) of the lasing spectrum was estimated to be 0.12 nm, which was denoted as $\delta\lambda$. Herein we cannot conclusively determine the narrowing of the laser line due to the spectral resolution limit of our spectrometer. According to the formula $Q = \lambda/\delta\lambda$ [12], the Q-factor of the PS-doped QD laser was calculated to be as high as 5218 ($\lambda = 626.15$ nm), which is twice as large as the Q-factors of the QD microbubble and microdisk lasers reported by Sun *et al.* in Refs. [6,7] and four times larger than that of the QD microplate laser reported by Rong *et al.* in Ref. [8]. In contrast to the lasing threshold of the pure QD laser, the increase in the lasing threshold of the PS-doped QD laser was due mainly to the reduction of the QD concentration caused by PS doping. It is worth mentioning that the threshold of the PS-doped QD laser was significantly lower than thresholds of the microbubble and microdisk lasers presented by Sun *et al.* in Refs. [6,7], as well as the previous QD lasers [13]. In order to demonstrate the enhancing effect of the ring microcavity host on lasing performance, we performed an additional experiment to characterize the random lasing characteristics of the same QDs, under comparable conditions. We found the lasing threshold of the QD random laser with comparable concentration was 150 μJ/mm^2. This value is 1100% higher than the lasing threshold of the PS-doped QD laser demonstrated in this work. It can be further improved by optimizing the quality of the nanocomposite film and engineering geometrical sizes of the annular grooves.

To analyze the photostability of the PS-doped QD microcavity laser, the lasing spectra were observed at different times. The photostability of a dye-doped microcavity laser was also characterized to benchmark the properties of the QD laser. Figure 4(a) shows the intensity stabilities of the PS-doped QD laser and Rhodamine 590-doped TZ001 polymer laser in air, under uninterrupted excitation. Herein the TZ001 is a hyperbranched polymer with a high RI (1.78). It possesses better adhesion compared to the PS on the surface of the etched annular groove. It may be of interest to note that the dye laser was fabricated using the same patterned wafer, demonstrating the versatility and reconfigurability of the external quasi-cavity

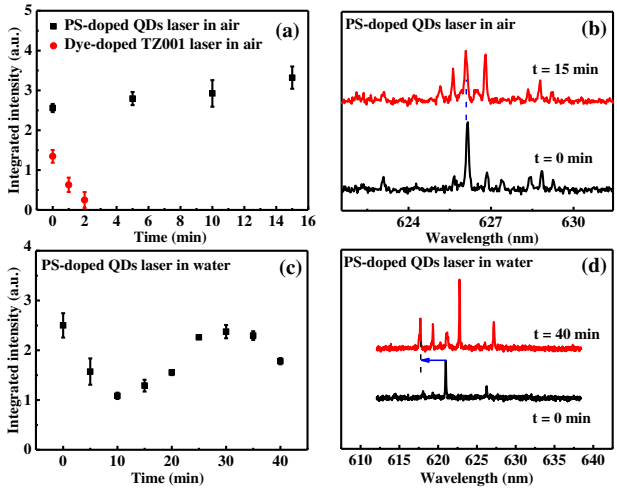

Fig. 4. Integrated intensity that expresses the stability over time of the PS-doped QDs and dye-doped TZ001 lasers in (a) air and (c) water for the PS-doped QD laser. Estimations of the lasing wavelength stabilities of the PS-doped QD laser in (b) air at $t = 0$ min and $t = 15$ min and in (d) water at $t = 0$ min and $t = 40$ min.

platform, as presented in our previous work [11]. The integrated intensity was recorded as one of the criteria of photostability, with the other criterion being the emission wavelength. By monitoring the laser emission over time, we can conclude that the integrated intensity of the QD laser was well-maintained over 15 min at a pump intensity of 31.56 μJ/mm^2. The integrated intensity of the dye laser, on the other hand, rapidly diminished within less than two minutes at an excitation intensity of 7.78 μJ/mm^2 (~2× the lasing threshold) due to photobleaching. In addition, cracks on TZ001 film increased the mode propagation loss. In fact, the excellent emission stability of the QD laser benefited from the high quantum efficiency and stable core–shell structure of the QDs [14], even when coated on the physically imperfect microcavity sidewalls. Figure 4(b) shows that the lasing wavelengths of the QD laser were relatively steady in air at time $t = 0$ min and $t = 15$ min. This adequately proves the stability of the laser emissions over time. When the QDs laser was immersed in water, the emission intensity fluctuated over time. Under the interrupted excitation mechanism, variations in the integrated intensities within 40 min were estimated with a time interval of 5 min at a pump intensity of 28.3 μJ/mm^2. For each measurement, three lasing spectra were collected to determine the error bar of the integrated intensity. The fluctuation of the intensity originated mainly from the appearance of the other modes in the integrated spectrum range, as shown in Fig. 4(c). The existence of these competing modes revealed the dynamic evolution of the lasing behaviors of the QD laser in water, primarily caused by the cracked surface morphology of the QD film on the wall of the ring resonator. The cracked QD film progressively absorbed water molecules, thereby modulating mode effective RI during the immersion time. Figure 4(d) shows that the lasing wavelengths were seriously blue-shifted in water from $t = 0$ to $t = 40$ min, which further demonstrated its instability under aqueous environment.

To explore the potentials of the QD laser for biosensing, the evolutions of the lasing wavelengths were monitored in real

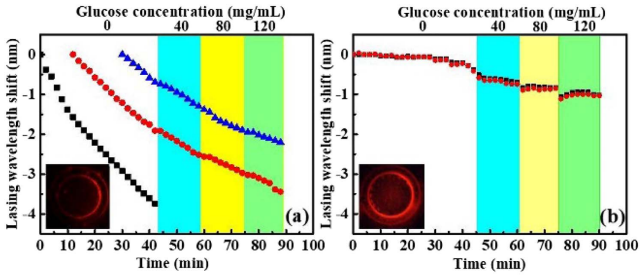

Fig. 5. Lasing wavelength shifts of the PS-doped QD microcavity lasers fabricated by (a) single spin-coating deposition (three modes represented by black, red, and blue curves), and by (b) two-step deposition process (two modes represented by red and black curves). The insets show the lasing light spots.

time with increasing glucose concentration at a pump intensity of 28.3 $\mu J/mm^2$. Glucose solution was selected due to its RI being linearly related to concentration. Furthermore, it does not cause any physical degradation to the QD film. Figure 5(a) shows the lasing wavelength shifts corresponding to three modes of the QD laser fabricated by the single spin-coating deposition process. The lasing wavelengths were blue-shifted as the glucose concentration in water was increased. This result seems to be contradictory to similar glucose sensing experiments using stable microcavity lasers, as the increase in glucose concentration typically shifts the wavelength to the red side of the spectrum. We have confirmed that the blue shifts occurred due to the glucose solution penetrating into the porous QD film throughout the entire experimental period. The penetrated glucose solution is more dominant than the increase in glucose concentration in lowering the mode effective RI. Therefore, the lasing wavelength drifted to the blue side of the spectrum over time. One of the modes denoted by a black dot disappeared when the 40 mg/mL glucose was injected. By recording the dynamics of the lasing spectra, two cavity modes denoted by red and blue dots in Fig. 5(a) were excited at $t = 12$ min and $t = 30$ min, respectively. While the glucose concentration was increased from 40 mg/mL to 120 mg/mL, these two modes showed similar trends in wavelength drifts as time progressed. However, the addition of glucose slightly decelerated the wavelength shift rates of both modes to the blue side. In addition, the large film stress caused the cracks in the QD film to keep growing. Since the rate of glucose volume increase in the QD film was dominant in comparison to that of glucose concentration increase, blue shifts were inevitable.

We attempted to improve the wavelength stability of the QDs microcavity laser in aqueous environment by engineering the quantum gain layer that was coated on the wall of the cavity host. A two-step deposition process was adopted to molecularly assemble the QD film. We experimentally varied the composition of QDs and PS dopant in the second film until we achieved lasing comparable to our previous experiments. We coated 15 mg/mL QDs with 1 wt. % of PS solution on the previous sample. Similarly, the lasing spectra were measured in real time at a pump intensity of 50.81 $\mu J/mm^2$. Figure 5(b) shows the wavelength shifts that correspond to two lasing modes. Notice that both lasing wavelengths were nearly constant within the first 35 min of the experiment. This improvement happened because the outer layer of the nanocomposite film was able to seal most of the cracks in the first gain layer and greatly reduced liquid penetration. Highly reduced blue shifts were still observed in the long-running experiment, as shown in Fig. 5(b). This was caused by the liquid that progressively penetrated into the imperfectly sealed gain layer. This imperfection can be further reduced by a more controllable second layer deposition technique, such as evaporation. The total wavelength shift in the two hours of experimentation was only about 1 nm. This was approximately 400% improvement in stability compared to the device without the outer layer coating [Fig. 5(a)]. Slight jumps in lasing wavelengths around the concentration borders were observed; they originated mainly from the competition of cavity modes. The lifetime of this on-chip QD laser has been demonstrated to be consistently longer than 90 min.

In conclusion, we have demonstrated an on-chip QD microcavity laser by molecularly engineering the quantum gain medium in the annular groove. The successful demonstration of a long-lifetime and stable on-chip QD microcavity laser in different environments will enable excellent micro-scale coherent light sources and diverse optical sensing applications in the near future.

Funding. National Natural Science Foundation of China (NSFC) (61805104, 61435006, 61525502); The Science and Technology Planning Project of Guangdong Province (2017B010123005).

†These authors contributed equally to this Letter.

REFERENCES

1. C. Dang, J. Lee, C. Breen, J. S. Steckel, and S. Coe-Sullivan, Nat. Nanotechnol. **7**, 335 (2012).
2. H. Kim, K. S. Cho, H. Jeong, J. Kim, C. W. Lee, W. K. Koh, Y. G. Roh, S. W. Hwang, and Y. Park, ACS Photon. **3**, 1536 (2016).
3. P. T. Snee, Y. H. Chan, D. G. Nocera, and M. G. Bawendi, Adv. Mater. **17**, 1131 (2005).
4. B. Min, S. Kim, K. Okamoto, L. Yang, A. Scherer, H. Atwater, and K. Vahala, Appl. Phys. Lett. **89**, 191124 (2006).
5. B. L. Feber, F. Prins, E. D. Leo, F. T. Rabouw, and D. J. Norris, Nano Lett. **18**, 1028 (2018).
6. Y. Wang, V. D. Ta, K. S. Leck, B. H. Tan, Z. Wang, T. He, C. D. Ohl, H. V. Demir, and H. D. Sun, Nano Lett. **17**, 2640 (2017).
7. Y. Wang, K. E. Fong, S. C. Yang, V. D. Ta, Y. Gao, Z. Wang, V. Nalla, H. V. Demir, and H. D. Sun, Laser Photon. Rev. **9**, 507 (2015).
8. K. X. Rong, C. W. Sun, K. B. Shi, Q. H. Gong, and J. J. Chen, ACS Photon. **4**, 1776 (2017).
9. A. Kiraz, Q. S. Chen, and X. D. Fan, ACS Photon. **2**, 707 (2015).
10. S. Pang, R. E. Beckham, and K. E. Meissner, Appl. Phys. Lett. **92**, 221108 (2008).
11. L. Wan, H. Chandrahalim, C. Chen, Q. S. Chen, T. Mei, Y. Oki, N. Nishimura, L. J. Guo, and X. D. Fan, Appl. Phys. Lett. **111**, 061109 (2017).
12. R. Chen, B. Ling, X. W. Sun, and H. D. Sun, Adv. Mater. **23**, 2199 (2011).
13. Y. Chen, J. Herrnsdorf, B. Guilhabert, Y. Zhang, I. M. Watson, E. Gu, N. Laurand, and M. D. Dawson, Opt. Express **19**, 2996 (2011).
14. C. Y. Cheng and M. H. Mao, J. Appl. Phys. **120**, 083103 (2016).